



HAL
open science

Full control of electric and magnetic light-matter interactions through a nanomirror on a near-field tip

Benoît Reynier, Eric Charron, Obren Markovic, Xingyu Yang, Bruno Gallas, Alban Ferrier, Sébastien Bidault, Mathieu Mivelle

► To cite this version:

Benoît Reynier, Eric Charron, Obren Markovic, Xingyu Yang, Bruno Gallas, et al.. Full control of electric and magnetic light-matter interactions through a nanomirror on a near-field tip. *Optica*, 2023, 10 (7), pp.841. 10.1364/OPTICA.486207. hal-04195064

HAL Id: hal-04195064

<https://hal.sorbonne-universite.fr/hal-04195064v1>

Submitted on 4 Sep 2023

HAL is a multi-disciplinary open access archive for the deposit and dissemination of scientific research documents, whether they are published or not. The documents may come from teaching and research institutions in France or abroad, or from public or private research centers.

L'archive ouverte pluridisciplinaire **HAL**, est destinée au dépôt et à la diffusion de documents scientifiques de niveau recherche, publiés ou non, émanant des établissements d'enseignement et de recherche français ou étrangers, des laboratoires publics ou privés.

1 **Full control of electric and magnetic light-matter**
2 **interactions through a nanomirror on a near-field tip**

3 **BENOIT REYNIER,¹ ERIC CHARRON,¹ OBREN MARKOVIC,¹ XINGYU YANG,¹**
4 **BRUNO GALLAS,¹ ALBAN FERRIER,^{2,3} SEBASTIEN BIDAULT⁴ AND MATHIEU**
5 **MIVELLE^{1*}**

6 ¹ *Sorbonne Université, Centre National de la Recherche Scientifique, Institut des*
7 *NanoSciences de Paris, 75005 Paris, France*

8 ² *Chimie ParisTech, Paris Sciences & Lettres University, Centre National de la*
9 *Recherche Scientifique, Institut de Recherche de Chimie Paris, 75005 Paris, France*

10 ³ *Faculté des Sciences et Ingénierie, Sorbonne Universités, UFR 933, Paris 75005,*
11 *France*

12 ⁴ *Institut Langevin, ESPCI Paris, Université PSL, CNRS, 75005 Paris, France*

13 **mathieu.mivelle@sorbonne-universite.fr*

14 **Abstract:** Light-matter interactions are often considered governed by the electric
15 optical field only, leaving aside the magnetic component of light. However, the
16 magnetic part plays a determining role in many optical processes from light and chiral-
17 matter interactions, photon-avalanching to forbidden photochemistry, making the
18 manipulation of magnetic processes extremely relevant. Here, by creating a standing
19 wave using a metallic nanomirror we manipulate the spatial distributions of the electric
20 and magnetic fields and their associated local densities of states, allowing the selective
21 control of the excitation and emission of electric and magnetic dipolar transitions. This
22 control allows us to image, in 3D, the electric and magnetic nodes and anti-nodes of
23 the fields' interference pattern. It also enables us to enhance specifically
24 photoluminescence from quantum emitters excited only by the magnetic field, and to
25 manipulate their spontaneous emission by acting on the excitation fields solely,
26 demonstrating full control of magnetic and electric light-matter interactions.

27 © 2023 Optica Publishing Group under the terms of the [Optica Publishing Group Open Access Publishing](#)
28 [Agreement](#)

29

30 **1. Introduction**

31

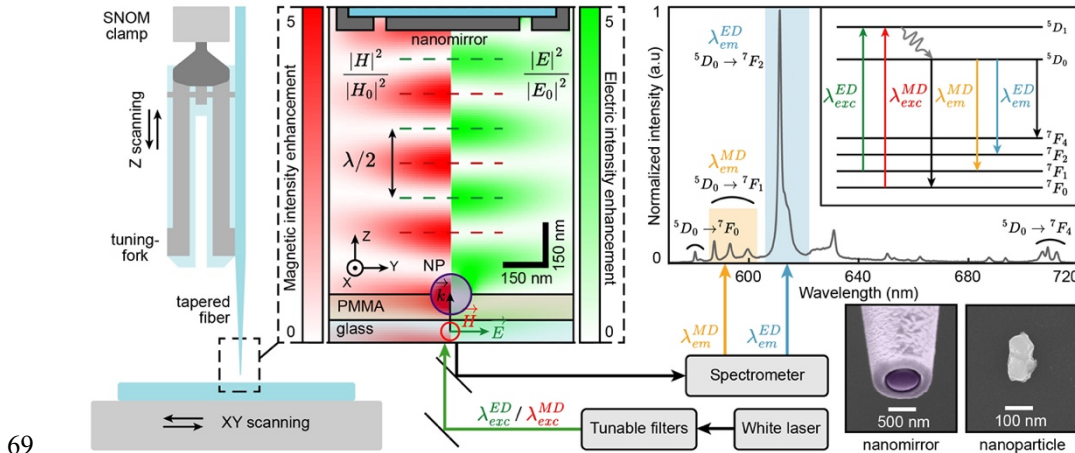
32 Manipulating light-matter interactions at the nanoscale has revolutionized many
33 scientific fields. Whether it be in biology, with ever more sensitive diagnostics
34 platforms [1, 2], medicine with targeted therapies [3, 4], chemistry with higher
35 efficiency catalysis [5, 6], or physical optics with ever more exotic manipulations of
36 these interactions [7-11]. Nevertheless, most of the systems developed to date have
37 aimed at manipulating the electric component of light, leaving aside its magnetic
38 counterpart. Indeed, light-matter interactions are often considered driven by the
39 electric optical field alone, ignoring the magnetic component of light. However, this
40 magnetic component plays a key role in many optical processes, such as chiral light-
41 matter interactions [12], ultrasensitive detection [13], enhancement of Raman optical
42 activity [14], photon-avalanching [15], or forbidden photochemistry [16], which
43 makes the manipulation of magnetic processes extremely important. Over the past few
44 years, several studies demonstrated a manipulation of specific ‘magnetic light’-matter
45 interactions. For instance, luminescence mediated by magnetic transition dipoles was
46 controlled and enhanced by manipulating the magnetic local density of states (LDOS)
47 through metallic layers acting as mirrors [17-22] or with resonant dielectric [23-32]
48 and plasmonic [33-36] nanostructures. It was also demonstrated that a Bessel beam
49 could selectively excite a magnetic dipole transition through the magnetic field of light
50 [37].

51 Here, we introduce a new platform made of a metallic nanomirror creating a standing
52 wave pattern to manipulate the spatial distributions of the electric and magnetic fields
53 and the associated LDOSes. With this platform, we demonstrate the selective
54 excitation of electric (ED) or magnetic (MD) dipolar transitions and selectively collect
55 the luminescence emitted by ED or MD transitions. This control allows us to image,
56 in 3D, the electric and magnetic nodes and anti-nodes of the fields’ interference
57 pattern. It also allows us to specifically enhance the luminescence of the quantum
58 emitter by magnetic excitation only and to manipulate the spontaneous emission of the
59 particle by acting on the excitation fields only, thus demonstrating total control of the
60 magnetic and electric light-matter interactions.

61

62 **2. Results**

63 For this purpose, a metallic nano-antenna is fabricated at the tip of an aluminum-coated
 64 tapered optical fiber (see Supplementary Materials 1) in a Scanning Near-Field Optical
 65 Microscope (SNOM) and acts as a nanomirror when excited from the far-field to create
 66 a standing wave (Fig. 1). This electromagnetic field is used to excite a Eu^{3+} doped Y_2O_3
 67 nanoparticle (see Supplementary Materials 1), whose position can be scanned at the
 68 nanoscale in 3D under the SNOM tip, allowing a dynamic control of the interactions.



69 **Fig. 1.** Principle of the experiment. A metallic nanomirror fabricated at the tip of a tapered
 70 fiber and placed on a SNOM (see Supplementary Materials 1) is brought near a Y_2O_3
 71 nanoparticle (NP) doped with Eu^{3+} ions. The excitation is performed by a spectrally
 72 tunable laser and the luminescence signal is collected using a spectrometer. Numerical
 73 simulations of the standing wave generated by the metallic nanomirror are displayed. The
 74 interferences of the magnetic intensity of the standing wave at λ_{exc}^{MD} are on the left side, in
 75 red, and those of the electric intensity at λ_{exc}^{ED} on the right side, in green. Both intensities
 76 are normalized by the amplitude of the incident field. The dotted lines are guides for the
 77 eye showing the spatial separation of the electric and magnetic anti-nodes in the standing
 78 wave. The purple circle indicates the Eu^{3+} -doped particle. The emission spectrum (for
 79 excitation at $\lambda_{exc}^{ED}=532$ nm) of Eu^{3+} ions in the Y_2O_3 matrix, with the magnetic and electric
 80 transitions of interest highlighted respectively in yellow and blue, is represented (see
 81 Supplementary Materials 1 for the emission spectrum when the particles are excited
 82 through the magnetic transition at $\lambda_{exc}^{MD}=527,5$ nm). The partial band diagram of Eu^{3+} ions
 83 shows the electric (λ_{exc}^{ED}) and magnetic (λ_{exc}^{MD}) transitions at the excitation and, respectively,
 84 at the emission (λ_{em}^{ED} , λ_{em}^{MD}).

86

87 Eu^{3+} ions are known to exhibit pure electric and magnetic transitions in the visible
88 spectrum, both in terms of excitation [37] and emission [18] (partial band diagram in
89 the inset of Fig. 1). The excitation of the ED (at $\lambda_{exc}^{ED} = 532$ nm) and MD (at $\lambda_{exc}^{MD} =$
90 527.5 nm) transitions is then performed by a white laser coupled to series of tunable
91 filters, allowing the reduction of the laser spectrum to a bandwidth of only 2 nm. This
92 bandwidth was chosen to minimize the crosstalk between electric and magnetic
93 excitations according to the excitation spectrum of Eu^{3+} ions (see Fig. S1 in the
94 Supplementary Materials). The luminescence of the ED (at $\lambda_{em}^{ED} = 610$ nm) and MD
95 (at $\lambda_{em}^{MD} = 590$ nm) transitions of the Eu^{3+} ions is then collected by the same objective,
96 filtered from the laser light, and measured by a spectrometer. The emission spectrum
97 of europium ions is shown in Fig. 1. By tuning the position of the nanoparticle within
98 the standing wave, we can thus selectively excite it with the E or H field and selectively
99 collect the signal emitted by the ED and MD transitions. Therefore, we have access to
100 the 3D distributions of the electromagnetic fields and of the local densities of optical
101 states that act on the quantum emitters (i.e. Eu^{3+}).

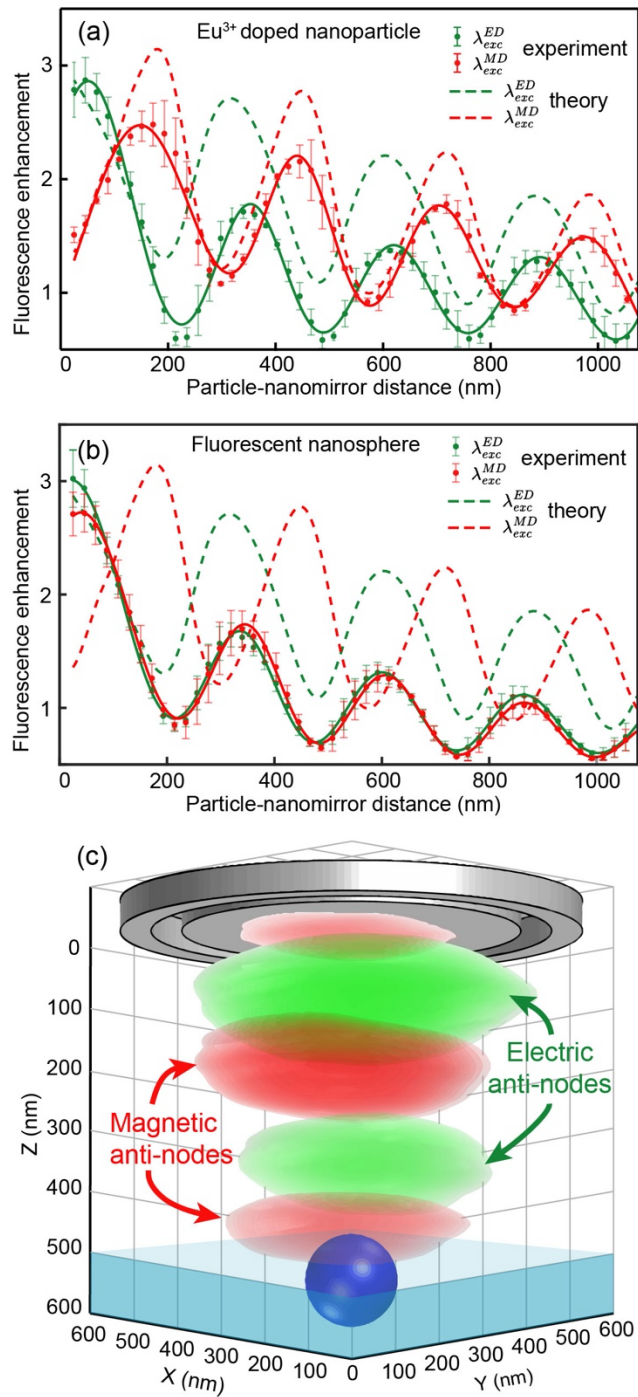
102 Fig. 1 shows the theoretical spatial distributions (see Supplementary Materials 2) of
103 the electric and magnetic fields generated by the standing wave beneath the metallic
104 nano-mirror at the λ_{exc}^{ED} and λ_{exc}^{MD} wavelengths, respectively. We observe that the
105 electric and magnetic nodes and anti-nodes do not overlap spatially. A maximum E
106 field corresponds to a minimum H field and vice versa. Furthermore, inside the anti-
107 nodes, the field intensities are increased by a factor of five compared to the incident
108 wave. Finally, due to the different continuity conditions at the interfaces, we can see
109 that the two components of light do not penetrate the doped nanoparticle in the same
110 way, with a clear predominance of the magnetic field inside the latter. Interestingly,
111 this means that the E and H excitations take place at slightly different positions within
112 the nanoparticle, as detailed further in the following paragraphs. Note that the
113 amplitudes of the maxima of the electric and magnetic fields are due to the
114 contributions of the reflection on the mirror, the gap between the nanodisc and the
115 aluminum on the surface of the tip, the presence of the substrate, and the increase of
116 the field within the particle. In particular, the presence of the particle and the substrate
117 influence the amplitude of the standing wave but not the position of its nodes and anti-

118 nodes (see paragraph 2 of the Supplementary Materials for the field maps of these
119 different conditions).

120 The luminescence intensity L of the europium-doped nanoparticle is proportional to
121 the average excitation intensity within the nanoparticle according to the following
122 equation: $L = \sigma|A|^2\eta Q$, where σ is the absorption cross-section, A is the electric or
123 magnetic excitation field, η is the collection efficiency, and Q the quantum yield. Fig.
124 2(a) provides the luminescence collected at λ_{em}^{ED} when exciting the particle at λ_{exc}^{ED} and
125 λ_{exc}^{MD} for different antenna-particle distances Z and normalized with respect to the
126 luminescence intensities without the nanomirror. We observe that the signals do not
127 overlap spatially: the maxima and minima for these two excitations are almost
128 inversed, in excellent agreement with the theoretical results expected from the
129 excitation of the particle by the E or H field of light (see paragraph 2 of the
130 Supplementary Materials for different particle geometries). These measurements thus
131 indicate that the evolution of L as a function of Z follows directly the evolution of the
132 excitation probability and that Q and η have a negligible influence on the spatial
133 distributions of the luminescence intensities. Importantly, since Q and η are
134 independent of the nature of the excitation process (MD or ED) and only depend on Z ,
135 it is possible to divide the luminescence enhancement measured at λ_{exc}^{ED} by the
136 luminescence enhancement measured at λ_{exc}^{MD} and recover directly the ratio between
137 the intensity enhancements of the E and H fields, providing a quantitative agreement
138 between measurements and theory (see Fig. S2 in Supplementary Materials 1). These
139 results also indicate that there is no spectral crosstalk between the two excitation
140 channels. Although, it should be noted that even if Q and η do not influence the spatial
141 distributions of the E and H fields, the difference in contrast between the theoretical
142 and experimental curves in Fig. 2a,b can be explained by the fact that the experimental
143 results, i.e., the number of photons collected, depend of the quantum yield of the
144 dipoles and the collection efficiency of our system. These quantities are not considered
145 in the theoretical results of Fig. 2a,b, which represent only the contributions of the
146 electric and magnetic fields within the particle. Moreover, the shape of the particles
147 can also influence this contrast (paragraph 2 of the Supplementary Materials).

148 As a control experiment, the measurement is also performed using a 200 nm diameter
149 nanoparticle filled with fluorescent molecules (Fig. 2(b), see Supplementary Materials

150 1). In this case, magnetic transitions are negligible compared to their electrical
151 counterpart, and the absorption spectrum overlaps with both the λ_{exc}^{ED} and λ_{exc}^{MD}
152 wavelengths (see Fig. S1 in Supplementary Materials 1). For fluorescent nanospheres,
153 the curves are perfectly superimposed, and the signal follows a purely electric
154 excitation. This measurement confirms that the luminescence collected in Fig. 2(a) for
155 a λ_{exc}^{ED} excitation represents the spatial distribution of the E field intensity in the
156 standing wave and that the signal for a λ_{exc}^{MD} excitation maps the magnetic field.
157 Furthermore, we observe that the fluorescence intensity is enhanced by a factor of 3
158 and 2.5 for, respectively, the excitation by the E and H fields compared to the signal
159 collected without the antenna. This measurement provides the first demonstration of
160 an enhanced luminescence signal from quantum emitters excited specifically by the
161 magnetic component of light.
162 Moreover, using the SNOM nano-positioning capabilities, the luminescence of Eu^{3+}
163 ions collected for each particle position in the volume under the nanomirror provides
164 a 3D spatial reconstruction of the E and H field intensities of the standing wave as
165 shown in Fig. 2(c). Here, the E and H nodes and anti-nodes are observed as lobes of
166 the standing wave because of the nanoscale size of the metallic mirror. This is the first
167 3D image providing, in parallel, the intensities of the electric and magnetic components
168 of light.
169
170
171



172

173 **Fig. 2.** Optical characterization of the standing wave. (a) Increase of the luminescence
 174 intensities emitted by the Eu³⁺-doped particle and collected by the spectrometer for
 175 excitation wavelengths at λ_{exc}^{ED} (in green) and λ_{exc}^{MD} (in red) and for different Z positions of

176 the particle under the nanomirror. (b) Increase in fluorescence intensity emitted from
 177 nanospheres filled with fluorescent molecules (see Supplementary Materials 1) for
 178 different Z positions under the nanomirror and excited at λ_{exc}^{ED} (in green) and λ_{exc}^{MD} (in red).
 179 In (a) and (b), the points correspond to the average values of the experimental data
 180 normalized by the signal without the antenna, the solid curves are polynomial fits serving
 181 as guides for the eye, and the dashed curves correspond to numerical calculations of the
 182 expected signal for an excitation by the magnetic field, in red, or the electric field, in green,
 183 of light. The error bars correspond to the standard deviation. (c) 3D image of the electric,
 184 in green, and magnetic, in red, nodes and anti-nodes of the electromagnetic standing wave
 185 generated under the nanomirror.

186

187 Finally, by tuning the excitation wavelength and studying separately the ED and MD
 188 emission intensities, we study how the metallic nano-mirror modifies the spontaneous
 189 emission rates for an electric or magnetic excitation. Since the emitted photons
 190 originate from the same excited state, we can infer the β^{ED} and β^{MD} branching ratios
 191 by considering any other transitions and non-radiative decay channels as losses [20]:

$$192 \quad \beta^{ED} = \frac{L^{ED}}{L^{ED} + L^{MD}} = 1 - \beta^{MD}, \quad (1)$$

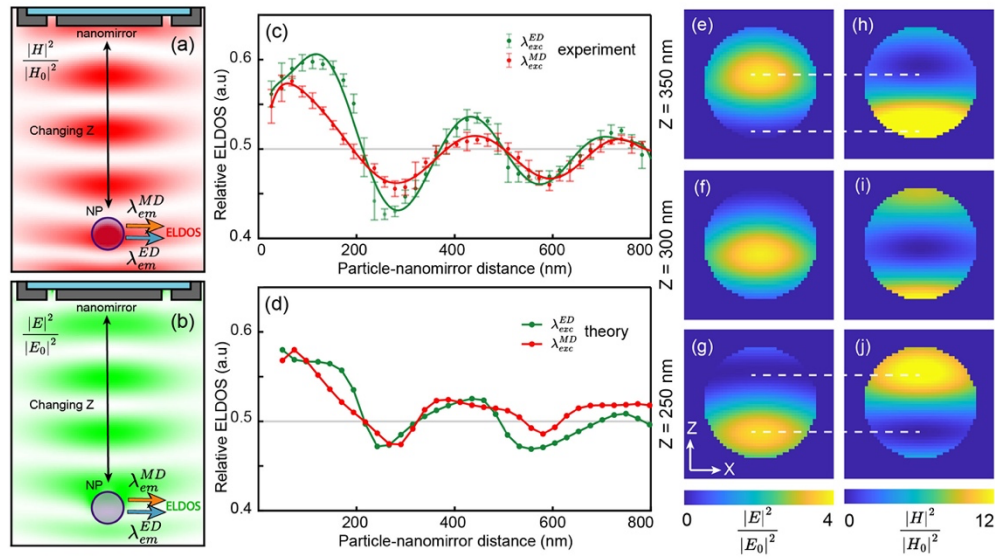
193 where L^{ED} and L^{MD} are respectively the luminescence signal emitted by the electric
 194 and magnetic transitions.

195 It is then possible to determine the relative local densities of states experienced by the
 196 ED (at λ_{em}^{ED}) and MD (at λ_{em}^{MD}) transitions as [20]:

$$197 \quad \tilde{\rho}^{ED} = \frac{\rho^{ED}}{\rho^{ED} + \rho^{MD}} = \frac{\beta_{NM}^{ED} / \beta_0^{ED}}{\beta_{NM}^{ED} / \beta_0^{ED} + \beta_{NM}^{MD} / \beta_0^{MD}} = 1 - \tilde{\rho}^{MD}, \quad (2)$$

198 with β_{NM} and β_0 representing the branching ratios with and without nanomirror,
 199 respectively. Fig. 3 provides the radiative electric LDOS when exciting the particle
 200 using the E or H field, respectively, for different nanomirror-particle distances.
 201 Interestingly, these two LDOSes, although measured at the same positions and thus in
 202 the same photonic environment, do not overlap spatially. The explanation can be found
 203 in the non-finite size of the Eu^{3+} doped nanoparticle. Indeed, depending on the
 204 component of light that interacts with the particle, the position of the excited ions will
 205 not spatially overlap because of a different spatial distribution of the fields within the
 206 particle as shown in Fig. 3e-j (see paragraph 2 of the Supplementary Materials for

207 different particle geometries). The emitting ions will therefore be at different positions
 208 corresponding to a different LDOS. Thus, by changing the nature of the exciting field,
 209 it is possible to turn on or off some ions and probe different spatial distributions of the
 210 LDOSes for electric and magnetic transition dipoles. These subtle variations are in
 211 good agreement with theoretical calculations when the LDOS, inferred from the
 212 photoluminescence measurements, is balanced by the distribution of the excitation
 213 fields within the particle (Fig. 3e-j).



214
 215 **Fig. 3.** LDOS change through field excitation. Principle of the experiment: The
 216 nanoparticle is excited by a) the magnetic field (at $\lambda_{exc}^{MD} = 527,5$ nm) or b) the electric field
 217 (at $\lambda_{exc}^{ED} = 532$ nm) for different mirror-particle distances. For each position, the number of
 218 photons emitted through the electric (at $\lambda_{em}^{ED} = 610$ nm) and magnetic (at $\lambda_{em}^{MD} = 590$ nm)
 219 channels are collected and used to calculate the relative Electric LDOS (ELDOS) via
 220 equations 1 and 2. (c) Experimental and (d) Theoretical relative electric LDOS as a
 221 function of the particle-nanomirror distance when the Eu^{3+} ions are excited at the resonance
 222 wavelength of the magnetic dipole transition, in red, or the electric dipole transition, in
 223 green. In (c) the solid curves are polynomial fits serving as guides for the eye and the error
 224 bars correspond to the standard deviation; $Z=0$ is chosen as the top part of the doped
 225 particle. Theoretical distribution of (e-j) electric (at λ_{exc}^{ED}) and (f-h) magnetic (at λ_{exc}^{MD})
 226 optical fields inside the nanoparticle, normalized by the incident wave and for different Z
 227 positions of the particle under the nanomirror (indicated on the left side). A mask is applied

228 to remove the fields outside of the particle for clarity, and the diameter of the nanoparticle
229 is 150 nm.

230 **3. Conclusion**

231 In conclusion, through a new platform, we demonstrated that by generating a standing
232 wave with a nanomirror at the end of a SNOM tip, we could perfectly control the
233 electric and magnetic interactions of light with quantum emitters, both in terms of the
234 excitation probability and of the spontaneous decay channels. This manipulation
235 allowed us to provide the first experimental 3D image of the electric and magnetic
236 nodes and anti-nodes of a standing wave. Furthermore, we demonstrated an increase
237 in the emission of a quantum emitter after specific excitation of its magnetic transition
238 dipole, and we showed how, by this full control of the interactions, we could, in
239 particular, manipulate the spontaneous emission of an emitter only by acting on the
240 nature (magnetic or electric) its excitation. This research opens the way to many
241 photonic applications involving a contribution from the optical magnetic field, such as
242 chiral light-matter interactions [12], photochemistry [16], manipulation of magnetic
243 processes [38], and new schemes in quantum computing [39] or nonlinear processes
244 [15], among others.

245 **Funding.** Financial support from the Agence national de la Recherche (ANR-20-CE09-0031-
246 01 and ANR-22-CE09-0027-04), from the Institut de Physique du CNRS (Tremplin@INP
247 2020) and the China Scholarship Council.

248

249 **Author Contributions.** M.M supervised the study. B.R, E.C and O.M performed the
250 experiments. B.R and X.Y performed the numerical study. A.F synthesised the Eu³⁺-doped
251 nanoparticles. B.R, B.G, S.B and M.M analysed the data. All the authors discussed the results
252 and contributed to writing the manuscript.

253

254 **Disclosures.** The authors declare no conflicts of interest.

255

256 **Data availability.** The data underlying the results presented in this paper are not publicly
257 available at this time but may be obtained from the authors upon reasonable request.

258

259 **Supplemental document.** See Supplementary Materials for supporting content and methods.

260 **References**

261

- 262 1. D. Punj, M. Mivelle, S. B. Moparthi, T. S. van Zanten, H. Rigneault, N. F.
263 van Hulst, M. F. García-Parajó, and J. Wenger, "A plasmonic 'antenna-in-box'
264 platform for enhanced single-molecule analysis at micromolar concentrations," *Nat.*
265 *Nanotechnol.* **8**, 512-516 (2013).
- 266 2. P. M. Winkler, R. Regmi, and V. Flauraud, "Antenna-based fluorescence
267 correlation spectroscopy to probe the nanoscale dynamics of biological membranes,"
268 *Nano. Lett.* **9**, 110-119 (2018).
- 269 3. D. P. O'Neal, L. R. Hirsch, N. J. Halas, J. D. Payne, and J. L. West, "Photo-
270 thermal tumor ablation in mice using near infrared-absorbing nanoparticles," *Cancer*
271 *letters* **209**, 171-176 (2004).
- 272 4. P. Fortina, L. J. Kricka, D. J. Graves, J. Park, T. Hyslop, F. Tam, N. Halas, S.
273 Surrey, and S. A. Waldman, "Applications of nanoparticles to diagnostics and
274 therapeutics in colorectal cancer," *Trends Biotechnol.* **25**, 145-152 (2007).
- 275 5. R. Grisel, K.-J. Weststrate, A. Gluhoi, and B. E. Nieuwenhuys, "Catalysis by
276 gold nanoparticles," *Gold Bulletin* **35**, 39-45 (2002).
- 277 6. R. Sardar, A. M. Funston, P. Mulvaney, and R. W. Murray, "Gold
278 nanoparticles: past, present, and future," *Langmuir* **25**, 13840-13851 (2009).
- 279 7. T. Taminiau, F. Stefani, F. Segerink, and N. Van Hulst, "Optical antennas
280 direct single-molecule emission," *Nat. Photonics* **2**, 234-237 (2008).
- 281 8. M. L. Juan, M. Righini, and R. Quidant, "Plasmon nano-optical tweezers,"
282 *Nat. Photonics* **5**, 349-356 (2011).
- 283 9. D. Akinwande, C. Huyghebaert, C.-H. Wang, M. I. Serna, S. Goossens, L.-J.
284 Li, H.-S. P. Wong, and F. H. Koppens, "Graphene and two-dimensional materials for
285 silicon technology," *Nature* **573**, 507-518 (2019).
- 286 10. J. J. Baumberg, J. Aizpurua, M. H. Mikkelsen, and D. R. Smith, "Extreme
287 nanophotonics from ultrathin metallic gaps," *Nat. Mater.* **18**, 668-678 (2019).
- 288 11. B. Yang, G. Chen, A. Ghafoor, Y. Zhang, Y. Zhang, Y. Zhang, Y. Luo, J.
289 Yang, V. Sandoghdar, and J. Aizpurua, "Sub-nanometre resolution in single-
290 molecule photoluminescence imaging," *Nat. Photonics* **14**, 693-699 (2020).

- 291 12. Y. Tang and A. E. Cohen, "Optical chirality and its interaction with matter,"
292 Phys. Rev. Lett. **104**, 163901 (2010).
- 293 13. Z. Xi and H. Urbach, "Magnetic Dipole Scattering from Metallic Nanowire
294 for Ultrasensitive Deflection Sensing," Phys. Rev. Lett. **119**, 053902 (2017).
- 295 14. T. Wu, X. Zhang, R. Wang, and X. Zhang, "Strongly enhanced Raman
296 optical activity in molecules by magnetic response of nanoparticles," J. Phys. Chem.
297 C **120**, 14795-14804 (2016).
- 298 15. C. Lee, E. Z. Xu, Y. Liu, A. Teitelboim, K. Yao, A. Fernandez-Bravo, A. M.
299 Kotulska, S. H. Nam, Y. D. Suh, and A. Bednarkiewicz, "Giant nonlinear optical
300 responses from photon-avalanching nanoparticles," Nature **589**, 230-235 (2021).
- 301 16. A. Manjavacas, R. Fenollosa, I. Rodriguez, M. C. Jiménez, M. A. Miranda,
302 and F. Meseguer, "Magnetic light and forbidden photochemistry: the case of singlet
303 oxygen," Journal of Materials Chemistry C **5**, 11824-11831 (2017).
- 304 17. N. Noginova, Y. Barnakov, H. Li, and M. Noginov, "Effect of metallic
305 surface on electric dipole and magnetic dipole emission transitions in Eu³⁺ doped
306 polymeric film," Opt. Express **17**, 10767-10772 (2009).
- 307 18. S. Karaveli and R. Zia, "Spectral tuning by selective enhancement of electric
308 and magnetic dipole emission," Phys. Rev. Lett. **106**, 193004 (2011).
- 309 19. T. H. Taminiau, S. Karaveli, N. F. van Hulst, and R. Zia, "Quantifying the
310 magnetic nature of light emission," Nat. Commun. **3**, 979 (2012).
- 311 20. L. Aigouy, A. Cazé, P. Gredin, M. Mortier, and R. Carminati, "Mapping and
312 quantifying electric and magnetic dipole luminescence at the nanoscale," Phys. Rev.
313 Lett. **113**, 076101 (2014).
- 314 21. R. Hussain, S. S. Kruk, C. E. Bonner, M. A. Noginov, I. Staude, Y. S.
315 Kivshar, N. Noginova, and D. N. Neshev, "Enhancing Eu³⁺ magnetic dipole
316 emission by resonant plasmonic nanostructures," Opt. Lett. **40**, 1659-1662 (2015).
- 317 22. F. T. Rabouw, P. T. Prins, and D. J. Norris, "Europium-Doped NaYF₄
318 Nanocrystals as Probes for the Electric and Magnetic Local Density of Optical States
319 throughout the Visible Spectral Range," Nano. Lett. **16**, 7254-7260 (2016).
- 320 23. B. Rolly, B. Bebey, S. Bidault, B. Stout, and N. Bonod, "Promoting magnetic
321 dipolar transition in trivalent lanthanide ions with lossless Mie resonances," Phys.
322 Rev. B **85**, 245432 (2012).

- 323 24. T. Feng, Y. Xu, Z. Liang, and W. Zhang, "All-dielectric hollow nanodisk for
324 tailoring magnetic dipole emission," *Opt. Lett.* **41**, 5011-5014 (2016).
- 325 25. D. G. Baranov, R. S. Savelev, S. V. Li, A. E. Krasnok, and A. Alù,
326 "Modifying magnetic dipole spontaneous emission with nanophotonic structures,"
327 *Laser & Photonics Reviews* **11**, 1600268 (2017).
- 328 26. T. Feng, W. Zhang, Z. Liang, Y. Xu, and A. E. Miroshnichenko, "Isotropic
329 magnetic Purcell effect," *ACS Photonics* **5**, 678-683 (2017).
- 330 27. M. Sanz-Paz, C. Ernandes, J. U. Esparza, G. W. Burr, N. F. van Hulst, A.
331 Maitre, L. Aigouy, T. Gacoin, N. Bonod, M. F. Garcia-Parajo, S. Bidault, and M.
332 Mivelle, "Enhancing magnetic light emission with all-dielectric optical
333 nanoantennas," *Nano. Lett.* **18**, 3481-3487 (2018).
- 334 28. A. Vaskin, S. Mashhadi, M. Steinert, K. E. Chong, D. Keene, S. Nanz, A.
335 Abass, E. Rusak, D.-Y. Choi, I. Fernandez-Corbaton, T. Pertsch, C. Rockstuhl, M. A.
336 Noginov, Y. S. Kivshar, D. N. Neshev, N. Noginova, and I. Staude, "Manipulation of
337 magnetic dipole emission from Eu³⁺ with Mie-resonant dielectric metasurfaces,"
338 *Nano. Lett.* **19**, 1015-1022 (2019).
- 339 29. P. R. Wiecha, C. Majorel, C. Girard, A. Arbouet, B. Masenelli, O. Boisron,
340 A. Lecestre, G. Larrieu, V. Paillard, and A. Cuche, "Enhancement of electric and
341 magnetic dipole transition of rare-earth-doped thin films tailored by high-index
342 dielectric nanostructures," *Appl. Opt.* **58**, 1682-1690 (2019).
- 343 30. X. Cheng, X. Zhuo, R. Jiang, Z. G. Wang, J. Wang, and H. Q. Lin,
344 "Electromagnetic Resonance-Modulated Magnetic Emission in Europium-Doped
345 Sub-Micrometer Zirconia Spheres," *Advanced Optical Materials* **9**, 2002212 (2021).
- 346 31. H. Sugimoto and M. Fujii, "Magnetic Purcell enhancement by magnetic
347 quadrupole resonance of dielectric nanosphere antenna," *ACS Photonics* **8**, 1794-
348 1800 (2021).
- 349 32. Y. Brûlé, P. Wiecha, A. Cuche, V. Paillard, and G. C. des Francs, "Magnetic
350 and electric Purcell factor control through geometry optimization of high index
351 dielectric nanostructures," *Opt. Express* **30**, 20360-20372 (2022).
- 352 33. S. M. Hein and H. Giessen, "Tailoring Magnetic Dipole Emission with
353 Plasmonic Split-Ring Resonators," *Phys. Rev. Lett.* **111**, 026803 (2013).

- 354 34. M. Mivelle, T. Grosjean, G. W. Burr, U. C. Fischer, and M. F. Garcia-Parajo,
355 "Strong Modification of Magnetic Dipole Emission through Diabolo Nanoantennas,"
356 ACS Photonics **2**, 1071-1076 (2015).
- 357 35. B. Choi, M. Iwanaga, Y. Sugimoto, K. Sakoda, and H. T. Miyazaki,
358 "Selective Plasmonic Enhancement of Electric-and Magnetic-Dipole Radiations of Er
359 Ions," Nano. Lett. **16**, 5191-5196 (2016).
- 360 36. C. Ernandes, H.-J. Lin, M. Mortier, P. Gredin, M. Mivelle, and L. Aigouy,
361 "Exploring the magnetic and electric side of light through plasmonic nanocavities,"
362 Nano. Lett. **18**, 5098-5103 (2018).
- 363 37. M. Kasperczyk, S. Person, D. Ananias, L. D. Carlos, and L. Novotny,
364 "Excitation of magnetic dipole transitions at optical frequencies," Phys. Rev. Lett.
365 **114**, 163903 (2015).
- 366 38. D. Bossini, V. I. Belotelov, A. K. Zvezdin, A. N. Kalish, and A. V. Kimel,
367 "Magnetoplasmonics and femtosecond optomagnetism at the nanoscale," Acs
368 Photonics **3**, 1385-1400 (2016).
- 369 39. D. Serrano, S. K. Kuppasamy, B. Heinrich, O. Fuhr, D. Hunger, M. Ruben,
370 and P. Goldner, "Ultra-narrow optical linewidths in rare-earth molecular crystals,"
371 Nature **603**, 241-246 (2022).
- 372
373